CT coreflood study of foam flow for enhanced oil recovery
The effect of oil type and saturation

Tang, Jinyu; Vincent-Bonnieu, Sebastien; Rossen, William R.

DOI
10.1016/j.energy.2019.116022

Publication date
2019

Document Version
Final published version

Published in
Energy

Energy 188 (2019) 116022

Contents lists available at ScienceDirect

Energy

journal homepage: www.elsevier.com/locate/energy

CT coreflood study of foam flow for enhanced oil recovery: The effect of oil type and saturation

Jinyu Tang [a, *], Sebastien Vincent-Bonnieu [a, b], William R. Rossen [a]

[a] Department of Geoscience and Engineering, Delft University of Technology, Stevinweg 1, Delft, 2628, CN, the Netherlands
[b] Shell Global Solutions International, 2288, Rijswijk, the Netherlands

ARTICLE INFO

Article history:
Received 20 May 2019
Received in revised form
14 August 2019
Accepted 26 August 2019
Available online 27 August 2019

Keywords:
Enhanced oil recovery
Foam flow with oil
CT corefloods
Simulation

ABSTRACT

We present a CT coreflood study of foam, both pre-generated and generated in-situ, displacing oil, as a function of oil type and saturation. Foam generation and propagation are reflected through sectional pressure measurements. Dual-energy CT imaging monitors in-time phase saturations. With an oil less harmful to foam (hexadecane), injection with and without pre-generation of foam exhibits similarities: propagation of a foam bank through a core and later refinement of foam texture. In contrast, with an oil destabilizing to foam (with 20 wt% oleic acid in the hexadecane), pre-generation of foam behaves very differently from co-injection, suggesting very-different effects on foam generation and propagation. Without pre-generation, strong-foam generation is very difficult even at residual oil saturation (about 0.1); generation finally starts from the outlet (likely a result of the capillary-end effect). This strong-foam state propagates upstream very slowly. Pre-generated foam shows two stages of propagation, both from the inlet to outlet. First, weak foam displaces most of the oil, followed by a propagation of stronger foam at lower oil saturation. This dependence on injection method with harmful oil is not represented in currently applied foam models, which need further improvements for reliable prediction of foam for enhanced oil recovery.

1. Introduction

Injection of gases (e.g., CO_2, steam, N_2 or hydrocarbon gases) is nowadays a mature enhanced oil recovery (EOR) technology [1–3]. Nevertheless, gas-injection EOR is in general subject to poor sweep efficiency [4]. Foam in porous media possesses unique microstructure (bubbles separated by interconnected thin liquid films) and reduces considerably gas mobility [5,6]. These features give foam injection into geological formations broad engineering applications, e.g. remediation of aquifers or soils [7,8] and carbon capture, utilization and storage [9–11]. In the petroleum industry, both laboratory studies and field pilots identify foam as a promising technology in assisting gas-injection EOR [6,12–14]. The application of foam for EOR mainly rests on the fact that the dramatic gas-mobility reduction caused by foam results in a remarkable increase in the sweep efficiency of gas injection and thus an increase in oil recovery. Key to the success of foam EOR is the effectiveness of foam for gas-mobility control, which is evaluated in terms of foam stability and strength (reflected through its apparent viscosity – the inverse of total relative mobility).

Foam-oil displacement in reservoirs is a complex process in which the effectiveness of foam is subject to many physical factors, e.g. water saturation, salinity, oil (saturation and composition), pressure, temperature, surfactant type and concentration, rock properties, etc. [6,15,16]. The impact of oil among these factors is prominent. Oil left in place after prior flooding is out of one's control and subsequent foam injection in most cases is unavoidably in contact with oils, most of which destabilize foam [15]. However, the quantitative correlation between foam stability and oil-related factors (e.g. oil saturation S_o and composition) has remained a long-standing challenge, in particular in transient displacements [15,16]. This gap in knowledge restricts our understanding to foam-oil interactions in geological formations and, more importantly, the reliable design of a foam EOR project.

Foam flow without oil at steady-state shows two regimes as a function of foam quality (i.e., gas volumetric fractional flow in foam) [17,18]: high- and low-quality regimes. Tang et al. [19,20] quantified the effect of several model oils on foam through their effects on the two foam regimes. Their data demonstrate that the

* Corresponding author.
E-mail address: J.Tang-4@tudelft.nl (J. Tang).

https://doi.org/10.1016/j.energy.2019.116022
0360-5442/

two regimes for steady-state foam flow without oil also apply to foam with oil, with the high-quality regime more sensitive to oil. In addition, they find in their data-fitting that the two foam regimes with oil can be captured by a widely used implicit-texture (IT) foam model, that in the STARS simulator [21]. These two regimes are often used as a starting point for deeper exploration of subsurface foam dynamics. In particular, the two regimes provide a basis for estimating foam model parameters in simulating foam EOR processes on the field scale (see, e.g. Refs. [22,23]). However, there is a knowledge gap concerning the transient dynamics of foam flow with oil and the confidence of using foam properties estimated from steady-state data to simulate dynamic displacement.

Many prior studies investigate transient foam flow with injection into a core initially at residual oil saturation S_{or} [24–27]. This S_{or} was achieved by pre-flushing an oil-saturated core with water and/or surfactant. In general, interpretation of results in such studies is complicated by the changing oil saturation during foam injection.

Recent studies explore the transient behavior of foam flow with oil using CT scanning to monitor phase distributions during coreflood [28,29]. In these studies, liquid-phase saturations were measured as a single saturation in the CT imaging. Foam stability without oil is controlled by the limiting capillary pressure, which corresponds to a limiting water saturation S_w^*, the water saturation below which foam collapses abruptly [30,31]. Tang et al. [19] show that oil destabilizes foam by increasing S_w^*. One cannot relate S_o to foam stability without distinguishing between the saturations of the two liquid phases (and, for instance, determining how close S_w is to S_w^*). More recently, Janssen et al. [32] investigate the creation of oil bank during foam injection, by measuring the three phase saturations separately. The model oil examined in this study is hexadecane, relatively less harmful to foam stability than some crude oils.

We present a CT coreflood study of foam displacement with two representative model oils: one benign to foam stability and the other very harmful to foam stability. A major purpose is to understand the transient dynamics of foam, both pre-generated and generated in situ by co-injection of surfactant solution and gas, as a function of oil (including oil type and oil saturation). We measure both transient and steady-state sectional pressure drops vs. time to infer foam properties and dynamics, e.g., generation, propagation and mobility. The real-time three saturation distributions along a core are monitored using dual-energy CT scanning. We then relate quantitatively foam properties and dynamics to phase distributions (in particular, oil type and saturation). At the end, we discuss the implications of the experimental findings to the engineering applications and simulations of foam EOR.

2. Experimental design

2.1. Materials and apparatus

2.1.1. Materials

For the purpose of the study, two representative model oils are examined: hexadecane (C_{16}), of 99% purity, supplied by Sigma-Aldrich, and a mixture of 80 wt% C_{16} and 20 wt% oleic acid (OA), of a purity 99%, provided by Honeywell Fluka. Their effects on steady-state foam flow have been shown in a recent study of Tang et al. [19]: C_{16} is relatively benign to foam stability, whereas the mixture with 20 wt% OA greatly destabilizes foam. Here we use these two model oils to examine the detrimental effects of oil on transient dynamics of in-situ-generated and pre-generated foam during EOR processes.

The gas phase is pure nitrogen (N_2) with a purity of 99.98%. The foaming agent is BIO-TERGE AS-40K AOS ($C_{14\text{-}16}$ alpha-olefin-sulfonate), delivered with an activity of 40%, used directly as received from the provider, Stepan company in USA. Surfactant solutions are prepared using deionized water. Surfactant concentration is 0.5 wt% AOS in the solution with 3 wt% sodium chloride (Merck). Below, for simplicity, aqueous surfactant solution is referred to as the water phase.

The core sample is Bentheimer sandstone. Table 1 lists the physical properties of the Bentheimer core sample used in our experiments. To avoid the complexity of property changes in core samples and facilitate the comparison of experimental results, we conduct all the measurements in the same core. Isopropanol of 99.9% purity (C_3H_8O, Emplura) is used to kill foam in cleaning the core.

2.1.2. CT coreflood apparatus

Fig. 1 shows a schematic of the CT coreflood apparatus for these experiments. As one follows the flow path starting from the left side, water and oil are each injected using a Vindum pump (VP-12K, Vindum Engineering, Inc.). The pump can work smoothly up to 12,000 psi (827.4 bar) and delivers oscillation-free flow rates ranging from 0.0001 to 29 cm^3/min. Two pistons in the pump allow continuous injection of water or oil at needed rates. Gas is provided by a 200-bar N_2 cylinder, and its injection is controlled through a Bronkhorst gas mass-flow controller (F-111B), with a rate ranging from 0.16 to 160 cm^3/min (at standard pressure P and temperature T conditions). The fluids are then injected into the Bentheimer core, which is within a PEEK (polyether-ether-ketone) coreholder. The core sample is sealed with a layer of glue about 0.2 cm thick, to prevent the bypass of fluids from the side of the core.

A back-pressure regulator is placed downstream of the coreholder to maintain P at the core outlet at 50 bar. Confining pressure, at the upstream injection pressure, is imposed by connecting the injection line to the narrow chamber between the coreholder and core sample, which is filled with water.

The whole coreflood apparatus is placed on the CT scanner table, the top portion of which is movable in both forward and backward directions. The pressure monitor records the pressure drops across six sections along the core through pressure transducers (i.e. $P_{1\text{-}7}$), with the first and last section of length 6.6 cm, and the four sections in the middle each of 6.7 cm. These transducers are connected to the Bentheimer core through the coreholder using PEEK tubes. The CT data monitor records CT measurements for phase distributions. The specifications of CT measurements and foam-flow experimental procedures are given in subsequent sections, with determination of phase distributions from CT images delineated in Appendix A.

2.2. CT measurements

CT scans in this study are taken perpendicular to flow direction and start from core outlet. Each slice scanned is 2 mm in thickness, with a resolution of 512 by 512 pixels. A single scan of the whole core comprises 204 slices, with two extra slices at each end of the core, and takes in total 27 s. CT numbers in foam flow with oil are a function of saturations of three phases: water saturation S_w, oil

Table 1
Physical properties of Bentheimer core used in foam flow experiments.

Properties	Quantities
Length (cm)	40±0.1
Diameter (cm)	4±0.1
Pore volume (cm^3)	110.5
Porosity (%)	22±0.1
Absolute permeability to brine (Darcy)	2.82±0.1

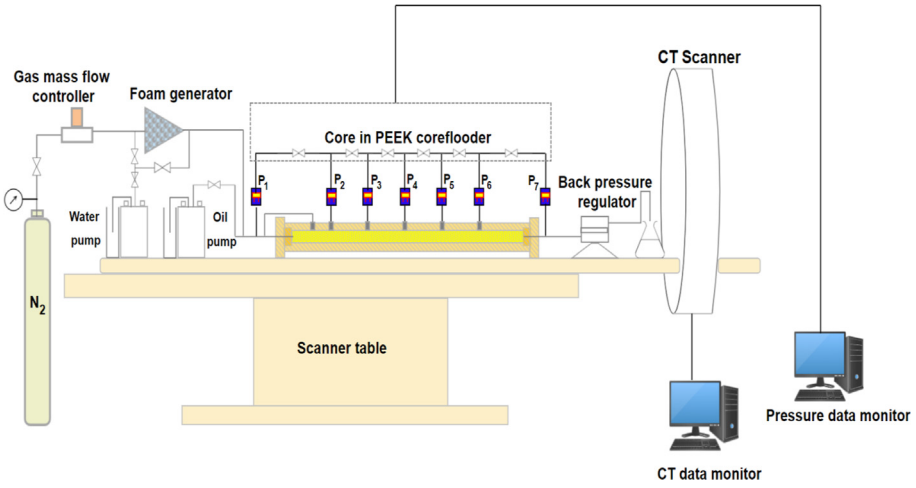

Fig. 1. Schematic of CT coreflood apparatus for foam-oil flow experiments.

saturation S_o and gas saturation S_g. To solve for S_w, S_o and S_g through measured CT numbers, one needs dual energies, each of which gives a series of independent CT numbers as a function of, e.g., S_w and S_o. S_g is then equal to $(1 - S_w - S_o)$. In our CT measurements, two beams, of energies 140 kv and 80 kv, are used.

To distinguish water from oil, a common practice is to dope either water or oil or both to enlarge the contrast in CT number between the two phases. 140-kv and 80-kv beams are employed in this study. Fig. 2 shows CT numbers of water doped by KI (potassium iodide) and oil doped by IDD (iododecane) in bulk, relative to cases without dopant. We find that doping the oil phase alone with 20 wt% IDD gives a greater contrast between CT attenuations (HU) of water and oil than doping water or both phases: 31 HU for water vs. 1012 HU for oil with 140 kv and 56 HU for water vs. 2386 HU for oil with 80 kv (seen from Fig. 2). Specifically, the CT attenuation ratio of 140 kv/80 kv for water (e.g., $31/56 = 0.55$) is different from that for doped oil (e.g., $1012/2386 = 0.42$). Therefore, the two energy beams yield two independent CT numbers in each voxel. Steady-state coreflood tests co-injecting gas, water and oil doped with 20 wt% IDD did not show noticeable difference in pressure gradient ∇P relative to that without oil dopant; this indicates the addition of IDD does not significantly affect foam behavior. We therefore choose to dope the oleic phase with 20 wt% IDD in our CT foam coreflood experiments. Note that 20 wt% OA examined is the mass concentration of OA in total oil mixture including dopant.

In the CT images we present below, red, green and blue represent 100%, 50% and 0% saturations of the given phase, respectively.

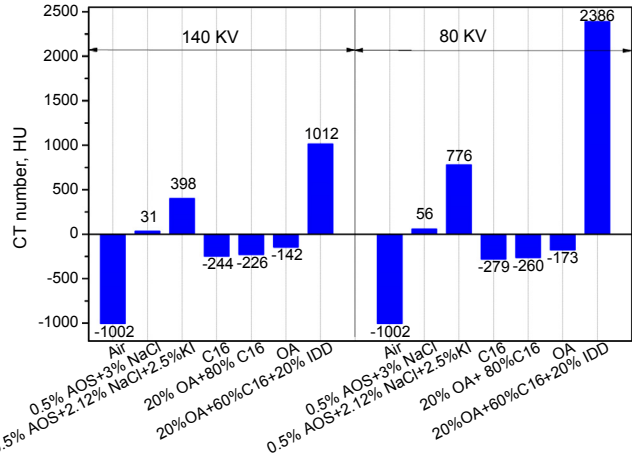

Fig. 2. CT numbers of water and oil in bulk with and without dopant at a temperature of 21 °C and pressure of 1 bar, in Hounsfield units (HU). IDD (iodododecane) is dopant for oil and KI (Potassium iodide), for surfactant solution. C_{16} and OA denote the model oils, hexadecane and oleic acid, and AOS is the surfactant used.

2.3. Experimental procedures

All the foam-oil flow experiments are conducted at ~21 °C. For the three-phase-saturation measurements using dual energies, one needs to follow a particular experimental sequence as follows. The specific formulas for calculating porosity and phase saturations based on measured CT numbers are described in Appendix A.

Step 1. Core sample preparation. Drill a Bentheimer core of size listed in Table 1. Apply a layer of glue to the radial surface of the core to prevent bypass of fluids along its side. Cut the glued core to fit the size of coreholder. Dry the core in an oven at 60 °C for 48 h. Insert the core into the coreholder and close the coreholder. Connect the coreholder to the rest of the apparatus and conduct gas-leakage test to ensure no leakage at elevated pressure. The following measurements are all with the back-pressure of 50 bar.

Step 2. CT scan of dry core (CT_{dry}). Conduct a CT scan of the dry core before introducing any liquids.

Step 3. CT scan of wet core (CT_{wet}) and permeability test. Conduct a CT scan of a 100% brine-saturated core, and measure the absolute permeability K of the core to brine.

Step 4. CT scan of the core at connate water saturation S_{wc} to oil flood (CT_{Swc}). Flush the brine-saturated core from Step 3 with 4 pore volumes (PV) oil until S_{wc} is reached (no more water production) and take a CT scan. Our measured value of S_{wc} is comparable to SCAL (Special Core Analysis) data in Bentheimer sandstone, i.e. 0.14–0.18 [33].

Step 5. CT scan of the core at S_{orw} (waterflood residual oil saturation) (CT_{Sorw}). Flush the core at S_{wc} in Step 4 with 4 PV brine and take a scan. The oil saturation with 4 PV injection of brine is at waterflood residual oil saturation S_{orw}; this is confirmed by lack of any visible oil production up to 15 PV injection.

Step 6. Injection of 1 PV surfactant solution to satisfy surfactant adsorption before foam injection. Because this is not an ultralow-IFT surfactant, no oil is produced during this step.

Step 7. Pressure-drop (ΔP) measurements and CT scan of the core during foam injection. Following Step 6, inject foam into the core at S_{orw} in one of two ways: either by co-injection of surfactant solution and gas or by direct injection of pre-generated foam. Upon injection, measure sectional ΔP vs. time and take CT scans according to foam responses that are reflected by the measured ΔP. Take a CT scan of the core at final steady state.

Step 8. Cleaning of the core sample:

- Kill foam from previous experiments using 4 PV isopropanol.
- Flush the core with CO_2 for 5 h. Most isopropanol is displaced out and the rest is volatized by CO_2, to guarantee no interference of isopropanol to following foam measurements.
- Clean CO_2 with >3 PV brine injection. Most CO_2 is displaced and the rest is dissolved in brine and flushed out of the core with brine through enhancing and releasing back pressure of 50 bar several times during the flush.
- Check the cleaning by measuring core permeability K to brine. If K deviates significantly from the original value, repeat the three previous cleaning steps. In our measurements, K after cleaning is within 7% of the original permeability; therefore we did not repeat the steps.

Step 9. Preparation of next experiment. Since the same core is used in additional experiments, Steps 2 to 4 give the reference CT scans that can be applied to three-phase saturation measurements in all subsequent experiments. Thus, in each new experiment, we prepare the core and satisfy surfactant adsorption following Steps 3 to 6, repeating the CT scan in Step 5 to determine S_{orw}, and then start foam injection and CT scans from Step 7.

3. Results and discussion

Table 2 gives an overview of the injection and initial conditions in each foam-oil coreflood. The experimental results include data on sectional ΔP along a core, saturations profiles and CT images. The data on ΔP quantify foam properties and reflect foam generation and propagation. Phase distributions obtained in CT measurements provide complementary data.

3.1. Model oil − C_{16}

3.1.1. In-situ-generated foam

Studies on foam flow with less-harmful oils, e.g. C_{16}, have been reported in the literature [28,33]. For comparison with foam flow with harmful oils, we refer to the results of Simjoo and Zitha [28] to illustrate the transient dynamics of in-situ-generated foam displacing C_{16}.

Fig. 3a, from Simjoo and Zitha [28], shows MRF (mobility reduction factor) upon co-injection of surfactant solution and gas into a core at waterflood residual saturation of C_{16}. They define MRF as the ratio of overall pressure drop with foam to that of brine flowing at 100% water saturation. Fig. 3b is the liquid-saturation (water plus oil) profile for the case with a surfactant concentration of 0.5 wt%. The rapid increase in MRF for this surfactant concentration demonstrates that with oil benign to foam stability strong foam could be generated immediately upon co-injection of gas and surfactant solution. Nevertheless, 2 PV foam injection is required before strong foam fills the core. A delay in strong foam filling the core is reported in prior studies (e.g. Refs. [27,34,35]).

Note that at steady state (e.g. 15.64 PV in Fig. 3a), liquid saturation remains greater near the inlet, thought to reflect an "entrance effect" in foam injection, where gas and water approach the final local-equilibrium foam. Water and oil are plotted together in the CT images of Simjoo and Zitha. It is difficult in their data to relate MRF to oil saturation or determine if an oil bank is created by

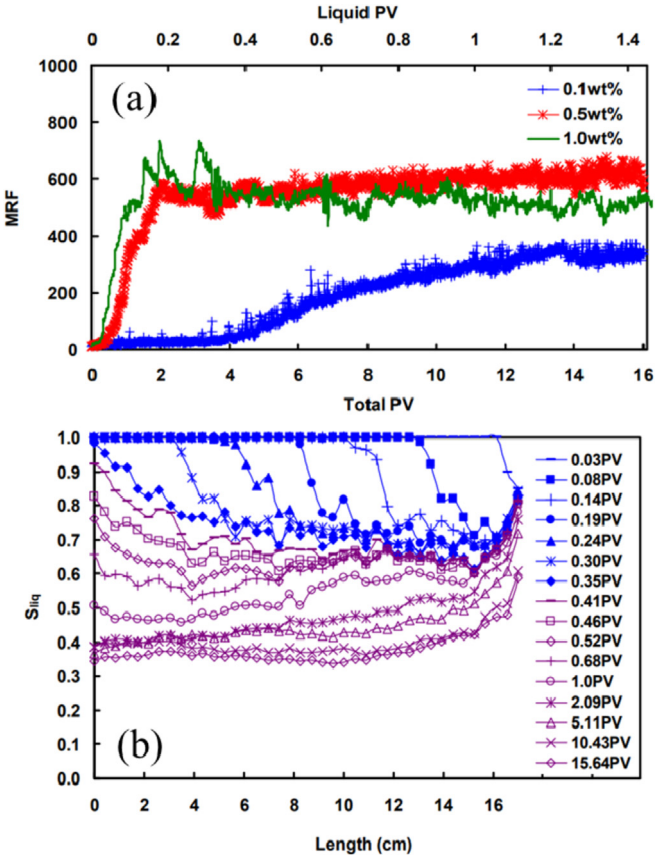

Fig. 3. Data from Simjoo and Zitha [28] on foam displacement with model oil C_{16} in a Bentheimer core initially at S_{orw}: (a) MRF (mobility-reduction factor); (b) liquid-saturation profile vs. position for the case with 0.5 wt% surfactant concentration. The right side of this plot corresponds to the core inlet. The injection and initial conditions are listed under EXP-01 in Table 2.

Table 2
An overview of experimental conditions in foam-oil flow experiments.

Experiment	Oil type	Injection condition			Initial condition (S_{orw})	Back pressure (bar)	Remarks
		f_g	u_t (ft/D)	Foam injection			
EXP-01	Hexadecane (C_{16})	91%	4.58	In-situ-generated foam	0.46±0.02	25	Simjoo and Zitha [28]
EXP-02		70%	4.58	Pre-generated foam	0.41±0.02	50	–
EXP-03	Mixture of 80 wt% C_{16} + 20 wt% OA	70%	4.58	In-situ-generated foam	0.39±0.02	50	–
EXP-04		70%	4.58	Pre-generated foam	0.45±0.02	50	–

OA denotes oleic acid; f_g (i.e., the gas fractional flow in foam) is the injected foam quality; $u_t = u_g + u_w$.

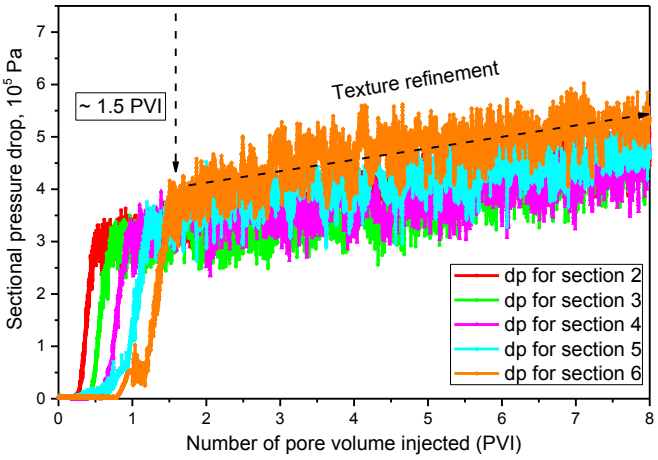

Fig. 4. Sectional pressure drops vs. PVI upon injection of pre-generated foam into a Bentheimer core at S_{orw} with C_{16}. dp denotes sectional pressure drop, with sections 1–6 numbered from core inlet to outlet. dp for section 2, obscured behind the other data, rises to about 4.85×10^5 Pa. The injection and initial conditions are listed under EXP-02 in Table 2.

foam.

3.1.2. *Pre-generated foam*

In our own experiment in the presence of C_{16}, pre-generated foam exhibits similarities in transient behavior to the case of in situ generation, as shown in Fig. 3. Fig. 4 presents sectional pressure-drop (dp) history during injection of pre-generated foam into a core initially with C_{16} at S_{orw}. Upon injection, strong foam propagates in the forward direction through the core over about 1.5 PV injection; this is comparable to the 2 PV injection (PVI) required to attain strong foam with in-situ generation in Fig. 3a. This is followed by an apparent refinement of foam texture, with sectional pressure drops at steady state increasing by about 42%. This refinement appears to take place simultaneously throughout the core. Similar refinement is also seen in the results of Simjoo and Zitha as in Fig. 3a and b, after foam breakthrough at about 0.4 PV.

The similarities between foam with and without pre-generation, e.g. propagation of foam bank and later refinement of foam texture, suggests that C_{16} has similar effects on foam generation and propagation. Similar effects might be expected for crude oil with components less-harmful to foam stability, such as heavy oils [15]. This argument is supported by experimental observations of in-situ foam generation in a recent study on steam foam with heavy oils [1].

Fig. 5 shows the three phase-saturation profiles as a function of dimensionless position and associated CT images (at the top) at different pore volumes injected, corresponding to the experiment in Fig. 4. Fig. 5a shows that foam in the forward propagation creates an oil bank with $S_o \approx 0.8$ at the displacement front. Nearly 50% OOIP (Oil Originally In Place) is produced through the oil bank by the initial foam propagation, with an additional 25% OOIP produced by the refined foam, leaving 25% OOIP in place (Fig. 5c).

S_g ~0 ahead of the foam front seen from gas saturation profiles and CT images in Fig. 5a and b suggests that foam effectively prevents gas from escaping ahead of the foam bank with the less-harmful oil. S_g remains at about 0.7 at steady state (shown in Fig. 5c), including both mobilized and trapped gas bubbles, but it is

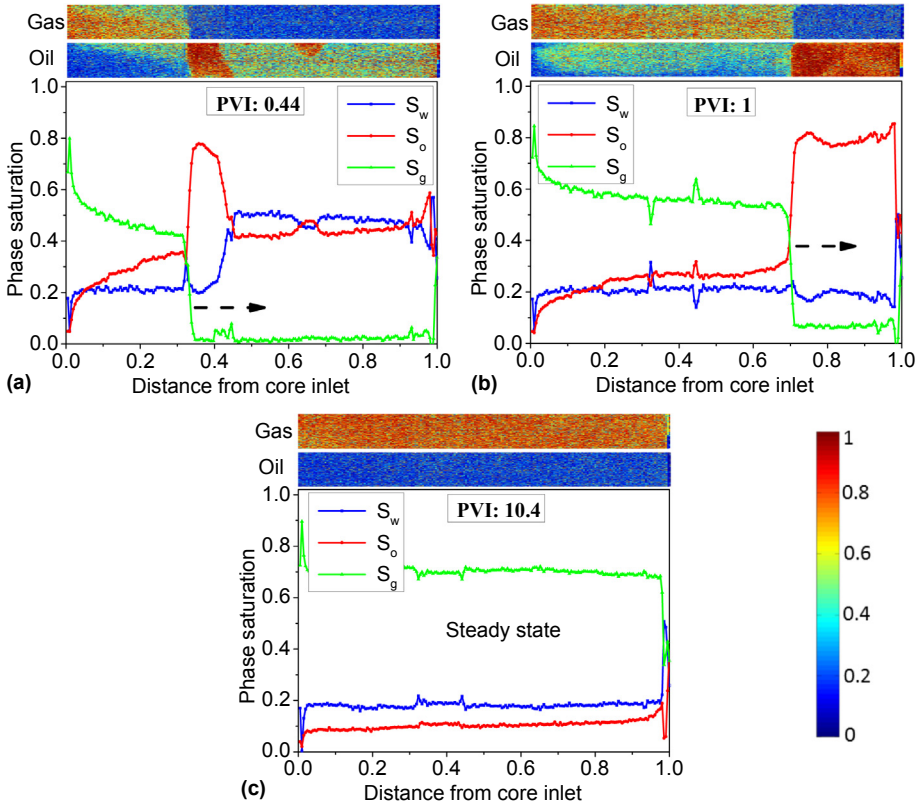

Fig. 5. Phase-saturation profiles vs. dimensionless position and CT-scan images (on top) for gas and oil, corresponding to the foam experiment of Fig. 4 at different times: **(a)** 0.44 PVI; **(b)** 1 PVI; **(c)** 10.4 PVI. Foam is injected from position zero. Arrows indicate the direction of foam propagation.

unclear of the proportion of each. The original water phase does not play a significant role in oil displacement; it is mainly displaced ahead of the oil bank rather than by foam.

3.2. Model oil – mixture of 80 wt% C_{16} and 20 wt% OA

With the presence of the model oil containing 20 wt% OA, foam generated in situ upon co-injection of phases behaves very differently from pre-generated foam.

3.2.1. In-situ-generated foam

Fig. 6 displays the sectional pressure-drop history upon co-injection of gas and water to develop in-situ foam in the Bentheimer core initially at S_{orw}. In this case the model oil contains 20 wt% OA; Fig. 6b is a continuation of Fig. 6a at later times. As seen from Fig. 6a and b, sectional pressure drops along the core do not show a significant increase except for that in the last section. Generation of strong foam begins near the core outlet. From about 25 to 40 PVI, the last sectional pressure drop keeps on rising but the others upstream remain nearly unchanged. We ended the experiment before seeing significant upstream propagation to the rest of

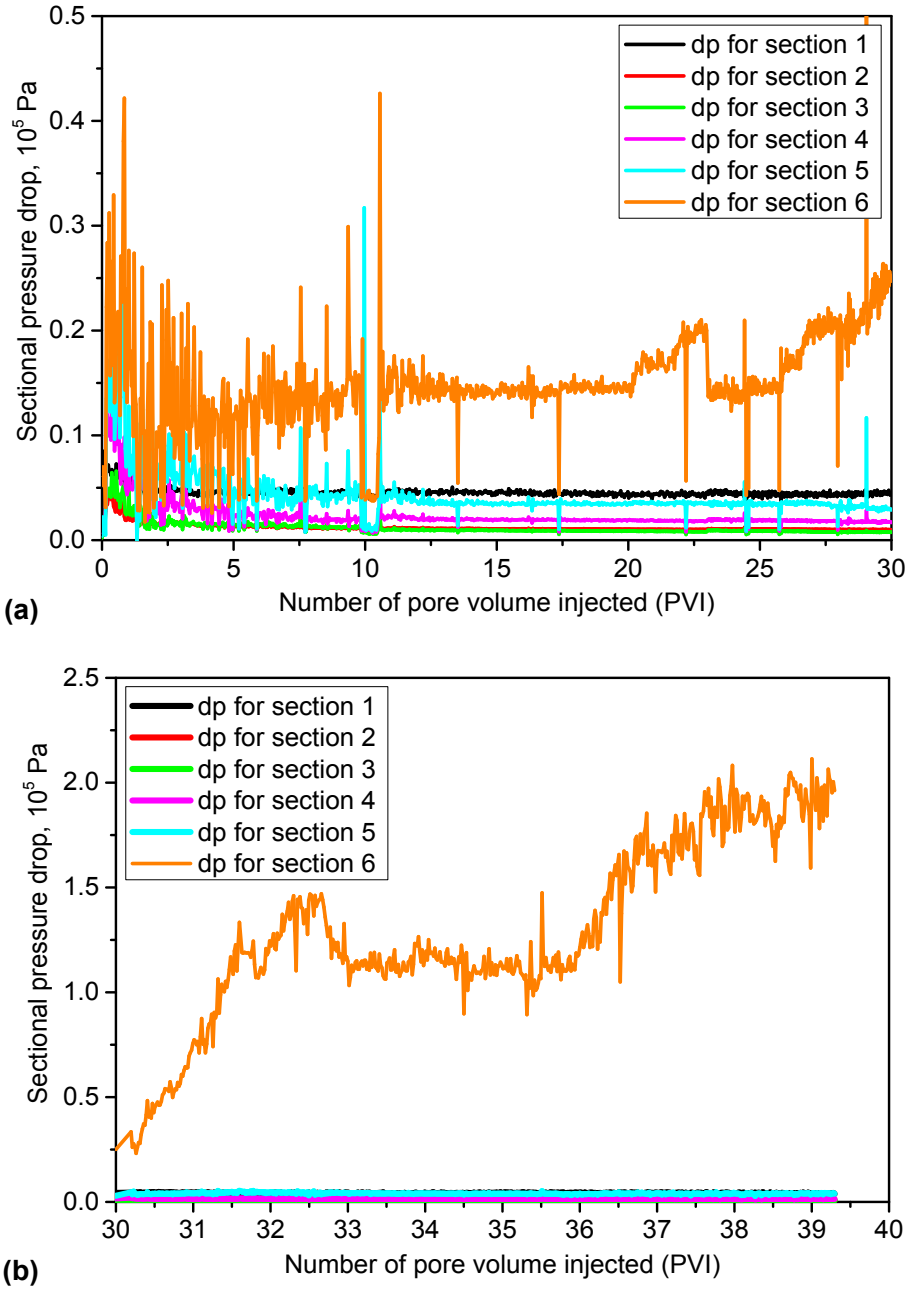

Fig. 6. Sectional pressure drops vs. PVI upon co-injection of gas and surfactant solution into a Bentheimer core at S_{orw}, with model oil comprising 80 wt% C_{16} and 20 wt% OA: **(a)** 0–30 PVI; **(b)** 30–40 PVI. dp denotes sectional pressure drop, with sections 1 to 6 numbered from core inlet to outlet. The injection and initial conditions are listed under EXP-03 in Table 2.

the core that is reported in other studies [36,37].

The generation of strong foam near the core outlet is thought to be triggered by the capillary-end effect, i.e. that capillary pressure drops sharply to zero at the outflow face of the core [37]. Similar behavior is reported by Shah et al. [39], where foam is generated due to capillary effects as flow crosses a sharp boundary between low and high permeabilities. Nevertheless, capillary-end effect that occurs on a lab scale is still of uncertain relevance to the field scale.

Fig. 7 gives the three phase-saturation profiles and CT images for gas and oil phases at different times for the experiment in Fig. 6. Saturation profiles in Fig. 7a suggest that prior to 0.69 PVI gas breakthrough has occurred, without displacing much oil or forming strong foam (Fig. 6a). In the second scan, taken at 33 PVI (Fig. 7b), the high gas saturation near the core outlet is consistent with the presence of strong foam there, indicated in Fig. 6b. Very close to the outflow face of the core in Fig. 7b, both water and oil saturations rise sharply, whereas gas saturation drops sharply, which is an indication of capillary-end effect; this suggests strong-foam generation is triggered by this effect.

Comparison of the gas- and water-saturation profiles near dimensionless position 0.8 in Fig. 7b and c suggest very slow, if any, backward propagation of strong foam. Such backward propagation is reported in the study of Apaydin and Kovscek [37] and of Nguyen et al. [38], both without oil. We very roughly estimate a dimensionless propagation rate of order 0.001 to 0.002. After 33 PVI (in Fig. 7b), residual oil saturation is relatively uniform along the core at about 0.1, but foam generation still does not occur except at the core outlet. This oil very detrimental to foam significantly restrains foam generation even at low saturation.

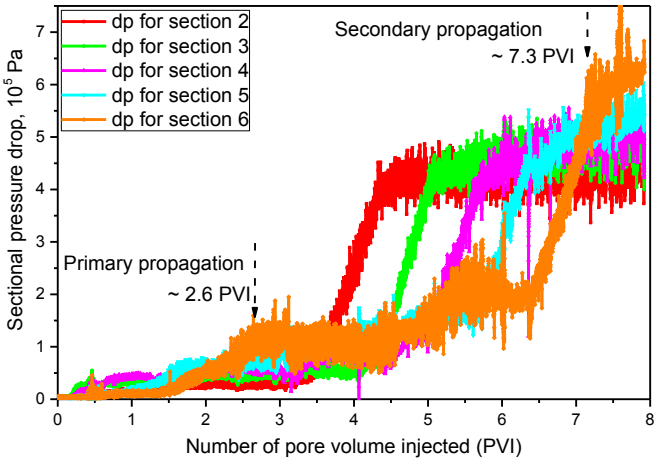

Fig. 8. Sectional pressure drops vs. PVI upon injection of pre-generated foam into a Bentheimer core at S_{orw}, with model oil comprising 80 wt% C_{16} and 20 wt% OA. dp denotes sectional pressure drop, with sections 1 to 6 numbered from core inlet to outlet. The injection and initial conditions are listed under EXP-04 in Table 2.

3.2.2. Pre-generated foam

Fig. 8 presents the sectional pressure-drop history upon direct injection of pre-generated foam into a Bentheimer core at S_{orw} with 20 wt% OA in the model oil. The evolution of sectional pressure drops suggests two stages of foam propagation. These two stages of propagation both start from the core inlet and march towards to the core outlet, as implied by the sequential increase in the sectional

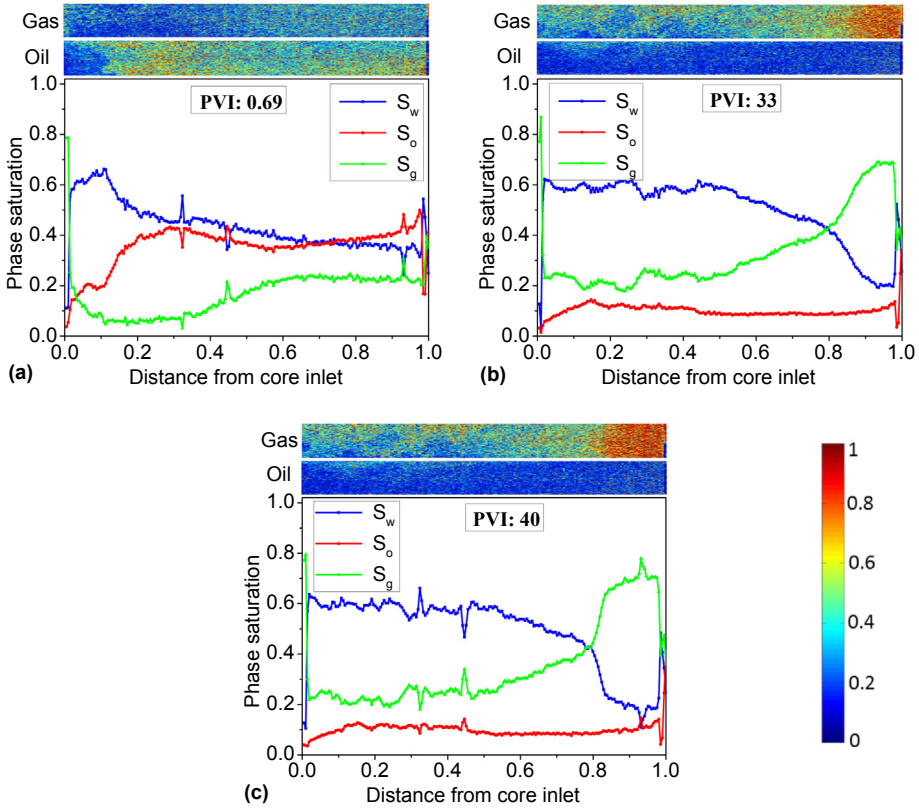

Fig. 7. Phase-saturation profiles vs. dimensionless position and CT scan images (on top) for gas and oil, corresponding to the foam experiment of Fig. 6 at different times: **(a)** 0.69 PVI; **(b)** 33 PVI; **(c)** 40 PVI. Foam is injected from position zero.

pressure drops from sections 2 to 6. Foam strength in sections 2 to 6 at 7.3 PVI in the second propagation wave increases respectively by a factor 5.2, 7.0, 8.4, 9.8 and 15.2 in the various sections, relative to the strength at 2.6 PVI during the initial propagation of foam.

The initial propagation of foam through section 6 takes 2.6 PVI, as seen in Fig. 8. The pressure drop for the first section was not recorded due to a limitation of the apparatus, so it is difficult to determine the starting time of the second propagation. It enters section 2 after more than 4.3 PVI.

Fig. 9 shows the associated phase-saturation profiles and CT images for gas and oil at different times for the experiment of Fig. 8. The measured saturations and CT images in Fig. 9a and b show that most oil (~74% OOIP) is displaced by the initial weaker foam, followed by the second, stronger foam that displaces a small quantity of oil (~3.8% OOIP). Gas distribution appears to be heterogeneous through the first 1.57 PVI, as seen from the gas CT images. Fig. 9b suggests the secondary propagation has started before the primary propagation reaches the core outlet. Upon injection, an ultimate residual oil saturation of about 0.1 (i.e. 22.2% OOIP) remains in place (Fig. 9c).

In the region between the first and second propagation fronts shown in Fig. 9b, although water saturation is relatively high, no strong foam is observed. Evidently, as suggested in Figs. 6 and 7, the presence of detrimental oils even at residual oil saturation about 0.1 inhibits the generation of stronger foam. The cause of the propagation of the second, stronger foam is unclear. Oil saturation was reduced somewhat in the stronger-foam front, but most of the oil was displaced ahead of the first front.

The combined results of the corefloods with and without pre-generation suggest that generating foam in absence of oil, either in the near-well region or in the wellbore, may be needed to ensure long-distance foam propagation in reservoirs with crude oil destabilizing foam. In the presence of residual oil, it may be very difficult to create foam.

3.3. Implications for foam EOR and modeling

3.3.1. Implications for applications of foam EOR

Manrique et al. [40] report that 377 out of 1507 worldwide EOR projects implement gas injection. In principle, those EOR projects that utilize gas injection are also applicable for foam injection, through which sweep efficiency can be significantly enhanced as well as oil recovery. To ensure successful engineering applications of foam EOR, one must take into account foam-oil interactions in the targeted reservoirs.

The experimental investigation we present provides crucial insights on two major aspects concerned with foam EOR: selection of candidate oil reservoirs and project design. Rock and fluid properties in an oil reservoir are out of one's control. Oils in different reservoirs have different components and thus different destabilizing effects to foam stability [15]. Foam EOR works more suitably for reservoirs with less-harmful oils, e.g. heavy oils [1]. To mitigate the poor injectivity of pre-generated foam, co-injection of surfactant solution and gas or SAG (surfactant-alternating-gas) may successfully make in-situ foam [41] in presence of less-harmful oils and displace it efficiently.

For those reservoirs with oils greatly detrimental to foam stability, co-injection of phases or SAG may risk of failure of foam

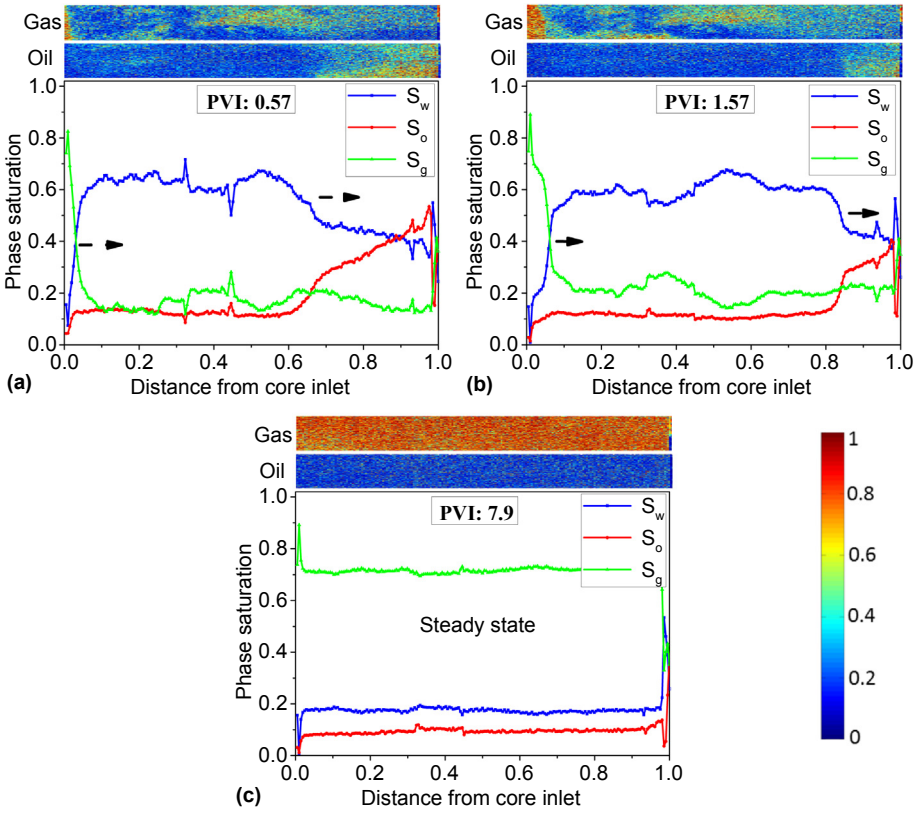

Fig. 9. Phase-saturation profiles vs. dimensionless position and CT-scan images (on top) for gas and oil, corresponding to the foam experiment of Fig. 8: **(a)** 0.57 PVI; **(b)** 1.57 PVI; **(c)** 7.9 PVI. Foam is injected from position zero. Arrows indicate the foam propagation direction.

generation in situ, which would lead to failure of foam EOR. The injection of foam pre-formed at surface or in the tubing may harm injectivity. In these situations, to develop in-situ foam with either co-injection of phases or SAG to displace oil, one needs to find surfactants or combinations of surfactants to enhance the tolerance of foam to oil. Experimental studies demonstrate that an abrupt transition from low to high permeability can assist in foam generation in the absence of oil [38,41,42,43]. If it is demonstrated to work in the presence of oil, another option could be to choose those oil reservoirs with large heterogeneity to apply foam EOR.

All of our experiments are conducted in water-wet conditions. A number of recent foam EOR field pilots are carried out in carbonate reservoirs [10,13], which are usually oil wet. Sanchez and Hazlett [44] conclude that foam cannot be generated in oil-wet formations with oil present, and that foam can be generated in oil-wet conditions without oil only when the formation wettability is altered by surfactant to water-wet. More efforts are needed to confirm the generality of their conclusions and understand the transient foam behavior (generation and propagation) in oil-wet reservoirs.

3.3.2. Implications for modeling of foam flow with oil

Foam EOR models reported in the literature in general fall into two groups [47]: population-balance models [44,45,46] and implicit-texture (IT) models [20,21,30]. Population-balance models represent explicitly the dynamic processes of foam creation and destruction and then represent gas mobility as a function of bubble size, or foam "texture". Such a model distinguishes between injection of pre-generated foam and co-injection of gas and water. However, these models are at an early stage of development in incorporating the effect of oil on foam [24,27,48]. Most numerical simulations of foam EOR processes are conducted with implicit-texture models. These models do not represent foam texture explicitly.

A widely used IT foam model, representative of current IT models, is the one in STARS simulator [21]. Foam in the IT model is represented through an overall mobility reduction factor *FM*, which reduce gas relative permeability [20], as follows:

$$k_{rg}^{f} = k_{rg}^{nf} \cdot FM, \tag{1}$$

$$FM = FM(S_w, S_o), \tag{2}$$

where k_{rg}^{f} and k_{rg}^{nf} represent gas relative permeability with and without foam, respectively, and *FM* is a function of only saturations S_w and S_o. The representation of foam in Eq. (1) and Eq. (2) is based on the "local-equilibrium (LE)" assumption, where foam properties characterized by the factor *FM* reach immediately its final state that corresponds to given (S_w, S_o).

Current simulations assume the LE assumption applies for all cases regardless of oil type and the manner of foam injection, and use directly foam-simulation parameters estimated from steady-state data to predict dynamic foam displacements with oil. Our experimental observations with less-harmful oils such as C_{16} and other prior studies without oil [49,50] support the application of the IT model to steady-state behavior.

However, IT foam models cannot distinguish the different results for co-injection of phases and direct injection of pre-generated foam as seen in Figs. 6 and 8. This finding does not depend on the details of the foam model. The reason is fundamental: IT foam models do not incorporate foam texture explicitly, but use a factor *FM* as in Eq. (2) to represent the apparent reduction in gas mobility by foam. Without accounting for foam texture, the two simulations would be simulated with identical injection conditions, which therefore would produce identical simulation results. It is possible that an IT model could represent either the case of co-injection or pre-generation on its own, but not both with the same parameters. This issue needs further exploration.

4. Conclusions

Foam interaction with oil in geological formations remains a long-standing challenge in foam enhanced oil recovery (EOR). We conduct a dual-energy CT coreflood study of foam flow with two representative model oils on the lab scale. Foam response and oil displacement are reflected by sectional pressure drops and phase-saturation distributions, respectively. The results provide initial insights for deeper exploration of foam-oil displacement and interactions on field scales.

The generation and propagation of foam is subject to the destabilizing effects of oil on foam and depends in part on the injection strategy. With oils less harmful to foam, e.g. C_{16}, pre-generated foam and in-situ-generated foam show similarities in transient dynamics: propagation of a foam bank through a core and later refinement of foam texture. This suggests that less-harmful oils have similar effects on foam generation and propagation. Analogous behavior could be expected for foam flow with heavy oils with compositions in general relatively benign to foam stability.

In contrast to less-harmful oils, very-detrimental oils (e.g. with 20 wt% oleic acid in our study) impose very different effects on the conditions for foam generation and propagation, as implied by the completely different behavior between the two manners of foam injection in our experiments. Foam generation in situ is very difficult with the harmful oil in place, even at low oil saturation. The initial generation of strong foam starts at the core outlet (thought to be a result of the capillary end effect) and propagates upstream. In contrast, pre-generated foam shows two stages of forward propagation from core inlet to outlet. The initial propagation comprises weak foam that displaces most of the oil, followed by the second propagation of stronger foam.

Implicit-texture foam models for EOR simulation cannot distinguish the different behavior between pre-generated and in-situ-generated foam, especially with very harmful oil. This finding does not depend on the details of the models. It is possible that such a model could represent one process or the other. Further investigations are on this issue and to improve the prediction of foam EOR.

Acknowledgements

This project is funded by the Joint Industry Project (JIP) on Foam for Enhanced Oil Recovery at Delft University of Technology. All authors thanks to Shell Global Solution for allowing to publish the findings in this study.

Appendix A. CT scan imaging of porosity and three-phase saturations using dual-energy

For the basics of CT scanning, one can refer to a prior study by Sharma et al. [51]. In our study, we implement beam energies of 140 kv and 80 kv, denoted by 1 and 2, respectively, in the following formulas.

Porosity is measured using single-energy beam 140 kv, calculated as follows:

$$\varphi = \frac{(CT_{wet})_1 - \left(CT_{dry}\right)_1}{CT_w - CT_a} \tag{A.1}$$

$(CT_{wet})_1$ = CT number of 100% brine saturated (wet) core at 140 kv, HU.

Substituting S_g in Eq. (A.4) into Eq. (A.2) and Eq. (A.3), we solve for expressions for saturations S_o and S_w:

$$S_o = \frac{\left[(CT_{wog})_1 - \left(CT_{dry}\right)_1\right]\left[(CT_{wet})_2 - \left(CT_{dry}\right)_2\right] - \left[(CT_{wog})_2 - \left(CT_{dry}\right)_2\right]\left[(CT_{wet})_1 - \left(CT_{dry}\right)_1\right]}{\left[(CT_{oil})_1 - \left(CT_{dry}\right)_1\right]\left[(CT_{wet})_2 - \left(CT_{dry}\right)_2\right] - \left[(CT_{oil})_2 - \left(CT_{dry}\right)_2\right]\left[(CT_{wet})_1 - \left(CT_{dry}\right)_1\right]}, \tag{A.6}$$

$$S_w = \frac{\left[(CT_{oil})_2 - \left(CT_{dry}\right)_2\right]\left[(CT_{wog})_1 - \left(CT_{dry}\right)_1\right] - \left[(CT_{oil})_1 - \left(CT_{dry}\right)_1\right]\left[(CT_{wog})_2 - \left(CT_{dry}\right)_2\right]}{\left[(CT_{oil})_2 - \left(CT_{dry}\right)_2\right]\left[(CT_{wet})_1 - \left(CT_{dry}\right)_1\right] - \left[(CT_{oil})_1 - \left(CT_{dry}\right)_1\right]\left[(CT_{wet})_2 - \left(CT_{dry}\right)_2\right]}. \tag{A.7}$$

$(CT_{dry})_1$ = CT number of 100% air saturated (dry) core at 140 kv, HU.
CT_w = CT number of brine in bulk at 140 kv, HU.
CT_a = CT number of air in bulk at 140 kv, HU.

The initial state in each experiment we conduct is at waterflood residual oil saturation S_{orw}, which is determined using 140 kv beam energy by:

$$S_{orw} = \frac{(CT_{Sorw})_1 - (CT_{wet})_1}{(CT_{oil})_1 - (CT_{wet})_1}, \tag{A.2}$$

where:

$(CT_{Sorw})_1$ = CT number of core at S_{orw} at 140 kv, HU.
$(CT_{oil})_1$ = CT number of 100% doped-oil saturated core at 140 kv, HU.

During foam injection with oil, CT attenuation combines the effects of water, oil, gas and rock matrix. For each voxel, the expressions for CT number can be written as follows:

$$\left(CT_{wog}\right)_1 = (CT_{wet})_1 S_w + \left(CT_{dry}\right)_1 S_g + (CT_{oil})_1 S_o, \tag{A.3}$$

$$\left(CT_{wog}\right)_2 = (CT_{wet})_2 S_w + \left(CT_{dry}\right)_2 S_g + (CT_{oil})_2 S_o, \tag{A.4}$$

$$S_g = 1 - S_w - S_o, \tag{A.5}$$

where:

$(CT_{wog})_1$ = CT number of fluid saturated core involving three phases at 140 kv, HU.
$(CT_{wog})_2$ = CT number of fluid saturated core involving three phases at 80 kv, HU.
$(CT_{wet})_1$ = CT number of 100% brine saturated (wet) core at 140 kv, HU.
$(CT_{wet})_2$ = CT number of 100% brine saturated (wet) core at 80 kv, HU.
$(CT_{dry})_1$ = CT number of 100% gas saturated (dry) core at 140 kv, HU.
$(CT_{dry})_2$ = CT number of 100% gas saturated (dry) core at 80 kv, HU.
$(CT_{oil})_1$ = CT number of 100% doped-oil saturated core at 140 kv, HU.
$(CT_{oil})_2$ = CT number of 100% doped-oil saturated core at 80 kv, HU.

To measure CT_{oil}, one has to disconnect the core from the coreholder, completely dry it in an oven and then re-saturate the core with oil until $S_o = 100\%$. This will unavoidably change the original position of the core where reference CT scans are taken, e.g. CT_{dry} and CT_{wet}. In our CT measurements, to avoid this risk, we estimate CT_{oil} using a CT scan of the core at S_{wc} achieved by oil flood, as follows:

$$(CT_{oil})_1 = \frac{(CT_{swc})_1 - (CT_{wet})_1}{1 - S_{wc}}, \tag{A.8}$$

$$(CT_{oil})_2 = \frac{(CT_{swc})_2 - (CT_{wet})_2}{1 - S_{wc}}, \tag{A.9}$$

where S_{wc} obtained by material balance is 0.2±0.02 and

$(CT_{swc})_1$ = CT number of core at S_{wc} achieved by oil flood at 140 kv, HU.
$(CT_{swc})_2$ = CT number of core at S_{wc} achieved by oil flood at 80 kv, HU.

In our actual calculations of phase saturations, initial state S_{orw} is determined by replacing $(CT_{oil})_1$ in Eq. (A.2) with the right side of Eq. (A.8). Similarly, S_o and S_w in Eq. (A.6) and Eq. (A.7) are finally calculated by replacing $(CT_{oil})_1$ and $(CT_{oil})_2$ with the right sides of Eq. (A.8) and Eq. (A.9), respectively.

References

[1] Bagheri SR. Experimental and simulation study of the steam–foam process. Part 2: the effect of oil on foam generation. Energy Fuels 2017;31(3):2687–96. Mar.
[2] Van Bergen F, Gale J, Damen K, Wildenborg A. Worldwide selection of early opportunities for CO_2-enhanced oil recovery and CO2-enhanced coal bed methane production. Energy 2004;29(9–10):1611–21.
[3] Zuloaga P, Yu W, Miao J, Sepehrnoori K. Performance evaluation of CO_2 Huff-n-Puff and continuous CO_2 injection in tight oil reservoirs. Energy 2017;134:181–92.
[4] Orr FM. Theory of gas injection processes, vol. 5. Tie-Line Publications Copenhagen; 2007.
[5] Kovscek A, Radke C. Fundamentals of foam transport in porous media. CA (United States): Lawrence Berkeley Lab.; 1993.
[6] Rossen WR. Foams in enhanced oil recovery. In: Foams: theory, measurements, and applications. MaRcel Dekker; 1996. p. 413–64.
[7] Hayes TD. Foam transport process for in-situ remediation of contaminated soils. 2001.
[8] Hirasaki G, Miller C, Szafranski R, Lawson J, Akiya N. Surfactant/foam process for aquifer remediation. In: Presented at the International symposium on oilfield chemistry; 1997.
[9] Bui M, et al. Carbon capture and storage (CCS): the way forward. Energy Environ Sci 2018;11(5):1062–176.
[10] Alcorn ZP, et al. An integrated CO2 Foam EOR pilot program with combined CCUS in an onshore Texas heterogeneous carbonate field," in SPE-190204-MS. SPE; 2018. p. 24.
[11] Ren B, Duncan IJ. Reservoir simulation of carbon storage associated with CO_2

EOR in residual oil zones, San Andres formation of West Texas, Permian Basin, USA. Energy 2019;167:391–401.
[12] Andrianov A, Farajzadeh R, Nick MM, Talanana M, Zitha PLJ. Immiscible foam for enhancing oil recovery: bulk and porous media experiments," in SPE-143578-MS. SPE; 2011.
[13] Carpenter C. Integrated CO_2-Foam pilot in a heterogeneous carbonate field. SPE-0718-0072-JPT Jul. 2018;70(7):72–4.
[14] Patil PD, et al. CO2 Foam field pilot test in sandstone reservoir: complete analysis of foam pilot response," in SPE-190312-MS. SPE; 2018. p. 14.
[15] Farajzadeh R, Andrianov A, Krastev R, Hirasaki GJ, Rossen WR. Foam–oil interaction in porous media: implications for foam assisted enhanced oil recovery. Adv Colloid Interface Sci 2012;183–184:1–13.
[16] Rossen WR. Numerical challenges in foam simulation: a review," in SPE-166232-MS. SPE; 2013.
[17] Alvarez JM, Rivas HJ, Rossen WR. Unified model for steady-state foam behavior at high and low foam qualities," SPE-74141-PA. Sep. 2001.
[18] Osterloh WT, Jante Jr MJ. Effects of gas and liquid velocity on steady-state foam flow at high temperature," in SPE-*24179-MS*. SPE; 1992.
[19] Tang J, Vincent-Bonnieu S, Rossen W. Experimental investigation of the effect of oil on steady-state foam flow in porous media. SPE-194015-PA Feb. 2019;24(1):140–57.
[20] Tang J, Ansari MN, Rossen WR. Quantitative modeling of the effect of oil on foam for enhanced oil recovery. SPE-194020-PA Jun. 2019;24(3):1057–75.
[21] Computer modeling group (Calgary, Alberta, Canada), *STARS user's guide*. 2015 [See also GEM User's Guide].
[22] Rossen WR, Boeije CS. Fitting foam simulation model parameters for SAG foam applications," in SPE-165*282-MS*. SPE; 2013.
[23] Boeije CS, Rossen W. Fitting foam-simulation-model parameters to data: I. coinjection of gas and liquid," SPE-174544-PA. May 2015.
[24] Myers TJ, Radke CJ. Transient foam displacement in the presence of residual oil: experiment and simulation using a population-balance model. Ind Eng Chem Res Aug. 2000;39(8):2725–41.
[25] Jensen JA, Friedmann F. Physical and chemical effects of an oil phase on the propagation of foam in porous media," in *SPE-16375-MS*. SPE; 1987. p. 14.
[26] Schramm LL, Novosad JJ. Micro-visualization of foam interactions with a crude oil. Colloids Surf, A Jan. 1990;46(1):21–43.
[27] Raterman KT. An investigation of oil destabilization of nitrogen foams in porous media," in *SPE-19692-MS*. SPE; 1989. p. 11.
[28] Simjoo M, Zitha PLJ. Effects of oil on foam generation and propagation in porous media," in SPE-165271-MS. SPE; 2013.
[29] Simjoo M, Dong Y, Andrianov A, Talanana M, Zitha P. CT scan study of immiscible foam flow in porous media for enhancing oil recovery. Ind Eng Chem Res 2013;52(18):6221–33.
[30] Cheng L, Reme AB, Shan D, Coombe DA, Rossen WR. Simulating foam processes at high and low foam qualities," in SPE-5*9287-MS*. SPE; 2000.
[31] Zhou Z, Rossen WR. "Applying fractional-flow theory to foam processes at the 'limiting capillary pressure. SPE Adv Technol Ser 1995;3(1):154–62.
[32] Janssen MTG, Pilus RM, Zitha PLJ. A comparative study of gas flooding and foam-assisted chemical flooding in Bentheimer sandstones. Transp. Porous Media; 2019.
[33] Andrianov A, Farajzadeh R, Mahmoodi Nick M, Talanana M, Zitha PL. Immiscible foam for enhancing oil recovery: bulk and porous media experiments. Ind Eng Chem Res 2012;51(5):2214–26.
[34] Janssen MTG, Zitha PLJ, Pilus RM. Oil recovery by alkaline-surfactant-foam ASF Flooding: effect of drive foam quality on oil bank propagation," in SPE-190235-*MS*. SPE; 2018. p. 32.
[35] Bergeron V, Fagan ME, Radke CJ. Generalized entering coefficients: a criterion for foam stability against oil in porous media. Langmuir Jul. 1993;9(7):1704–13.
[36] Mannhardt K, Novosad JJ, Schramm LL. Foam/oil interations at reservoir conditions," in SPE-39681-*MS*. SPE; 1998.
[37] Apaydin OG, Kovscek AR. Surfactant concentration and end effects on foam flow in porous media. Transp Porous Media 2001;43(3):511–36.
[38] Nguyen QP, Rossen WR, Zitha PL, Currie PK. Determination of gas trapping with foam using X-ray computed tomography and effluent analysis. SPE J 2009;14(2):222–36.
[39] Shah SY, Wolf K-H, Pilus RM, Rossen WR. Foam generation by capillary snap-off in flow across a sharp permeability transition. In: Presented at the SPE improved oil recovery conference; 2018.
[40] Manrique EJ, et al. EOR: current status and opportunities," in *SPE-130113-MS*. SPE; 2010. p. 21.
[41] Gong J, et al. Modeling of liquid injectivity in durfactant-alternating-gas foam enhanced oil recovery. SPE J 2019. 190435-PA.
[42] Falls AH, Hirasaki GJ, Patzek TW, Gauglitz DA, Miller DD, Ratulowski T. Development of a mechanistic foam simulator: the population balance and generation by snap-off," SPE-14961-PA. Aug. 1988.
[43] Tanzil D, Hirasaki GJ, Miller CA. Mobility of foam in heterogeneous media: flow parallel and perpendicular to stratification. In: Presented at the SPE Annual Technical Conference and Exhibition; 2000.
[44] Sanchez J, Hazlett R. Foam flow through an oil-wet porous medium: a laboratory study. SPE Reserv Eng 1992;7(1):91–7.
[45] Kovscek AR, Patzek TW, Radke CJ. A mechanistic population balance model for transient and steady-state foam flow in Boise sandstone. Chem Eng Sci Dec. 1995;50(23):3783–99.
[46] Kam SI. Improved mechanistic foam simulation with foam catastrophe theory. Colloids Surf. Physicochem. Eng. Asp. Apr. 2008;318(1):62–77.
[47] Lotfollahi M, Farajzadeh R, Delshad M, Varavei A, Rossen WR. Comparison of implicit-texture and population-balance foam models. J Nat Gas Sci Eng 2016;31:184–97.
[48] Ma K, Mateen K, Ren G, Luo H, Bourdarot G, Morel D. "Mechanistic modeling of foam flow through porous media in the presence of oil: review of foam-oil interactions and an improved bubble population-balance model. In: Presented at the SPE Annual Technical Conference and Exhibition; 2018.
[49] Persoff P, Radke CJ, Pruess K, Benson SM, Witherspoon PA. "A laboratory investigation of foam flow in sandstone at elevated pressure," SPE-18781-PA. Aug. 1991.
[50] Kovscek AR, Chen Q, Gerritsen M. Modeling foam displacement with the local-equilibrium approximation: theory and experimental verification. SPE J 2010;15(1):171–83.
[51] Sharma BC, Brigham WE, Castanier LM, Reid T. CT imaging techniques for two-phase and three-phase in situ saturation measurements. Doctoral dissertation. Stanford University; 1997.